analytical chemistry

pubs.acs.org/ac

Article

MetaPhenotype: A Transferable Meta-Learning Model for Single-Cell Mass Spectrometry-Based Cell Phenotype Prediction Using Limited Number of Cells

Songyuan Yao,[§] Tra D. Nguyen,[§] Yunpeng Lan,[§] Wen Yang, Dan Chen, Yihan Shao,* and Zhibo Yang*

Cite This: *Anal. Chem.* 2024, 96, 19238−19247

Read Online

ACCESS | Metrics & More | Article Recommendations | Supporting Information

ABSTRACT: Single-cell mass spectrometry (SCMS) is an emerging tool for studying cell heterogeneity according to variation of molecular species in single cells. Although it has become increasingly common to employ machine learning models in SCMS data analysis, such as the classification of cell phenotypes, the existing machine learning models often suffer from low adaptability and transferability. In addition, SCMS studies of rare cells can be restricted by limited number of cell samples. To overcome these limitations, we performed SCMS analyses of melanoma cancer cell lines with two phenotypes (i.e., primary and metastatic cells). We then developed a meta-learning-based model, MetaPhenotype, that can be trained using a small amount of SCMS data to accurately classify cells into primary or metastatic phenotypes. Our results show that compared with standard transfer learning models, MetaPhenotype can rapidly predict and achieve a high accuracy of over 90% with fewer new training samples. Overall, our work opens the possibility of accurate cell phenotype classification based on fewer SCMS samples, thus lowering the demand for sample acquisition.

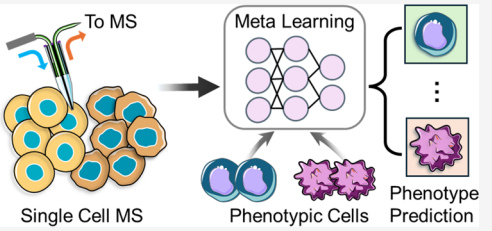

INTRODUCTION

Cell heterogeneity—a substantial variation in the cell appearance, behavior, biochemical capabilities, and gene expression profiles[1,2]—is a fundamental characteristic of living organisms. Arising from genetic diversity, environmental influences, and stochastic processes,[3−6] cell heterogeneity is of great significance in human health. Clinically, cell heterogeneity leads to cancer therapy response variations,[7−11] making it a leading cause of therapeutic cancer failure, including cancer spread, recurrence, and drug resistance.[12−15] As such, it has become increasingly common to consider cell heterogeneity in the development of new antitumor drugs, alternative cancer therapies, and treatment for other disorders.[16]

Phenotypic heterogeneity is a type of cell heterogeneity defined as cells with the same genetic background but different phenotypes. Phenotypic heterogeneity of cells have been observed in genetic systems and human diseases, and it is essential for disease diagnosis and treatment.[17] Melanoma cancer cells, for instance, exhibit as heterogeneous phenotypes (e.g., primary and metastatic phenotypes) when subjected to different microenvironment perturbations such as drug treatment.[7,18,19] Phenotypic heterogeneity of cells can be traced to alterations in their molecular profiles. For example, compared to primary cancer cells, differentially expressed protein biomarkers and metabolites have been observed in metastatic cancer cells (e.g., in melanoma,[20,21] pancreatic,[22] and breast[23] cancers). Discriminating cells with different phenotypes can improve our understanding of key biological processes in healthy and diseased tissues,[24−27] and facilitate the monitoring of the development, homeostasis, and course of diseases.

Modern mass spectrometry (MS) techniques are uniquely suited for studying cell metabolomic profiles and cell heterogeneity. Indeed, thousands of metabolites can now be detected simultaneously in MS experiments from cell samples. However, conventional bulk analysis cannot evaluate cell heterogeneity. To acquire metabolomic profiles of heterogeneous single cells and shine light into their biological pathways,[28,29] numerous single-cell mass spectrometry (SCMS) technologies have emerged recently.[30−46] Among them, the Single-probe SCMS technique is an ambient SCMS method that has been used for studies of live cells,[36,47−50] including the heterogeneity of parasite infection of cells,[51] differential metabolomic profiles of cells with drug resistance,[52,53] and variations in quantities of small molecules (e.g., anticancer drugs[54−58] and nitric oxide[59]) in single cells. In this work, the single-probe SCMS method was used to analyze single melanoma cancer cells with different phenotypes.

In tandem with the advancement of novel SCMS technologies, new data analysis methods are needed to effectively analyze the acquired data. While traditional

Received: April 18, 2024
Revised: October 29, 2024
Accepted: November 12, 2024
Published: November 21, 2024

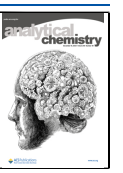

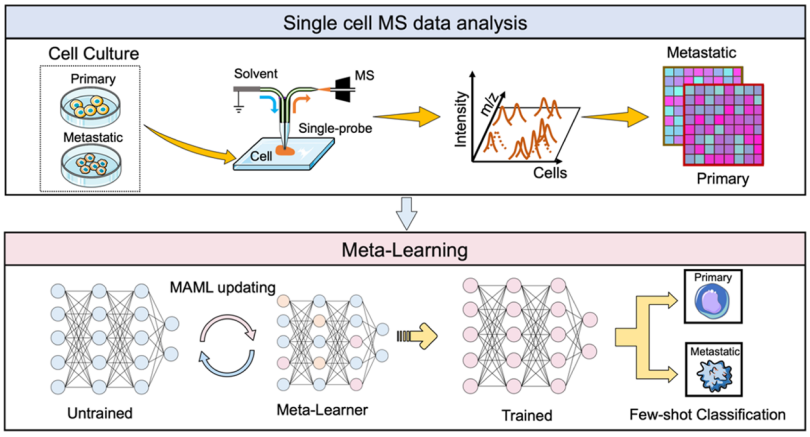

Figure 1. Workflow of combined Single-probe SCMS experiments and data analysis using the MAML-based machine learning model, MetaPhenotype.

statistical data analysis methods, such as *t* test and ANOVA (Analysis of Variance), are still used as important tools to analyze SCMS data (e.g., to determine species with significantly different abundances in cells from different groups), they are ill-suited to handling a large amount of data from SCMS experiments of cells with complex biological features. In their place, new machine learning-based methods have emerged to extract essential information from such big data, and guide the diagnosis,[60,61] prognosis,[54,60,62−64] and treatment[65−67] of cancers. In particular, a series of machine learning algorithms, including artificial neural network (ANN), support vector machine (SVM), principal component analysis (PCA), and random forest (RF) have been utilized in MS research.[68−70] Thanks to these developments, machine learning algorithms have been used increasingly to analyze MS data with a goal of developing a cancer diagnostic and biomarkers discovery platform for image data analysis,[71−74] single-cell classification,[54,55,68,75] and other applications.

However, machine learning applications in SCMS data analysis can become challenging in some cases. Conventional machine learning algorithms, particularly deep learning, generally requires large training (labeling) data sets to achieve a high-accuracy prediction.[18] They have been employed to analyze data generated from high throughout, vacuum-based SCMS experiments such as matrix enhanced (ME)-SIMS (e.g., ∼2000 cells)[76] and MALDI-TOF (e.g., 1544 cells).[77] However, most ambient-based methods require rather careful sample handling to minimize the environment perturbation on live cell metabolism, resulting in relatively smaller numbers of cells in each experiment. Some examples include as few as 108 cells from Single-probe SCMS,[55] 32 cells from microprobe CE-ESI-MS,[78] and 15 cells from nano-DESI MS.[79] In addition to the limitation of ambient SCMS techniques, the SCMS data size can be further limited by the availability of samples such as stem cells[49] and circulating tumor cells.[80] However, when limited data are available for training, conventional machine learning models can encounter overfitting: they perform well for the training data set, but make poorer predictions for actual sample SCMS data.[81] Thus, it is imperative to develop new machine learning models to utilize limited amounts of SCMS data and thereby improve the efficiency of data utilization.

To achieve this goal, it is desirable for us to leverage recent developments in Few-Shot Learning,[82] a new subfield of machine learning that seeks to generalize from few training examples. In practice, most few-shot algorithms are based on meta-learning.[83] Also known as "Learning to Learn,"[84,85] meta-learning starts from the "meta-learning stage," where one solves multiple similar tasks (such as classification) at the same time. This learning experience, thus, allows the resultant meta-learning model to be rapidly adapted in the "adaption stage" to handle new and similar tasks even with a few new training examples. As such, meta-learning is expected to be suitable for handling unseen tasks in SCMS studies with limited data, including identifying cell subgroups, discovering hidden structures of cells, and studying cell phenotypes (e.g., primary and metastatic cells) for future therapy.

Among various meta-learning methods, model agnostic meta-learning (MAML)[86] has been especially wide-used in many research areas, including image classification,[87] natural language processing (NLP),[88] and robotics.[89] Algorithm-wise, MAML stands out for its simplicity with only one set of model parameters. In essence, a MAML model is trained for some tasks using a small number of samples, and the trained model is then be adapted to a new task within a small number of optimization (such as gradient descent) steps.[86] The advantages and previous successful applications of the MAML algorithm opened the door for its use to analyze relatively small amounts of data from SCMS.

Nearly all existing MAML models employ convolutional neural network (CNN) algorithms in the meta-learning and adaptation stages. Different types of CNN models can be constructed to analyze data with different dimensionalities. For example, 1D-,[90−92] 2D-,[93,94] and 3D-CNN[95−97] models are used to extract features from 1D, 2D, and 3D data. To date, most MAML-based works utilize the architecture based on 2D-CNN, which is very effective in analyzing various 2D signals such as images. However, 1D-CNN, which is easier to train due to its less computational complexity,[93,98] would be clearly preferable for analyzing 1D signals, particularly when limited training data are available.[90] Recent studies demonstrated that 1D-CNN can indeed be used effectively in MS data analysis.[99] Specifically, 1D-CNN was employed in cumulative transfer learning to recognize patterns in a small MS data (e.g., train a data set with only two outputs and classify up to 12 output categories) to train a model and transfer this model to classify cell phenotypes.[99] As such, a 1D-CNN-based MAML approach for 1D-SCMS classification will constitute an exciting new area of application for MAML.

https://doi.org/10.1021/acs.analchem.4c02038
Anal. Chem. 2024, 96, 19238−19247

In this work, we constructed an MAML-based machine learning model, which is termed MetaPhenotype, and demonstrated its unique capabilities of classifying cell phenotypes based on SCMS data acquired from phenotypical melanoma cell lines (Figure 1). Our SCMS experiments were performed using the Single-probe technique. The cell line models used in this work included two different pairs of melanoma cell lines, and each cell pair is isogenic but has two different phenotypes: primary and metastatic cells. The SCMS experiments were conducted using cells with and without anticancer drug treatment. It was the first time that the MAML algorithm with a 1D-CNN architecture was utilized to construct a machine learning model for SCMS data analysis. This novel tool allowed us to achieve a rapid adaptation of the ML model using a limited amount of new training data from a small number of single cells. The trained model demonstrated remarkedly high transferability. Specifically, while the MetaPhenotype model was trained using one pair of primary/metastatic melanoma cell lines without drug treatment, it can be readily transferred to accurately classify the new data from cells, including the same pair of cell lines after drug treatment and a different pair of primary/metastatic melanoma cell lines (with and without drug treatment), into two phenotypes: primary and metastatic cells.

METHODS

Experiments. *Cell Culture.* Two pairs of melanoma cancer cell lines with different phenotypes, WM115 (primary)/WM266-4 (metastatic) and IGR39 (primary)/IGR37 (metastatic), were used as cell models. WM115 and WM266-4 cells were cultured in Dulbecco's Modified Eagle's Medium (DMEM, Santa Cruz Biotechnology Inc., Dallas, TX) supplemented with 10% fetal bovine serum (FBS, Life Technologies, Grand Island, New York) and 1% penicillin-streptomycin (Pen-Strep, Life Technologies, Grand Island, New York) in 5% CO_2 at 37 °C. IGR39 and IGR37 cells were cultured in Rosewell Park Memorial Institute 1640 Medium (RPMI, Thermo Fisher Scientific Inc., Waltham, Massachusetts) with 10% FBS and 1% Pen-Strep in 5% CO_2 at 37 °C.

Cells were cultured to reach 80% confluency at approximately 6×10^6 cells in 10 cm cultured dishes. After an overnight culture, trypsinization was performed to detach cells and then quenched with fresh completed DMEM or RPMI medium supplemented with 10% FBS and 1% Pen-strep for WM115/WM266-4 or IGR39/IGR37, respectively. The cell suspension was counted using a hemocytometer and diluted with fresh completed DMEM (with added 10% FBS and 1% Pen-Strep) to a concentration of 1×10^6 cells in 1 mL of cell media.

Vemurafenib Treatment. 12-well plates were used for cell treatment prior to SCMS experiments. A glass coverslip (18 mm in diameter) was placed in each well prior to adding cell suspension. Two mL of diluted cell suspension was added to each well in the 12-well plate. The plate was incubated for 18−24 h to enable cell attachment at 37 °C with 5% CO_2. Anticancer drug vemurafenib was dissolved in dimethyl sulfoxide (DMSO) to prepare the stock solutions, and then diluted to 1 μM in cell-containing wells. The cells were then treated with vemurafenib at 0.5 μM for 48 h. After 48 h treatment, the glass coverslips were removed from the 12-well plates and rinsed three times with fresh DMEM (no FBS and Pen-Strep Supplement) to eliminate all cell debris or residues before performing SCMS experiments. The control cells were also incubated for 48 h and subjected to analysis (Figure S1). The cells were kept in fresh DMEM (no FBS and Pen-Strep Supplement) during the experiment to ensure that the single cells were alive.

Single-Probe SCMS. The Single-probe SCMS setup consists of a Single-probe, two digital microscopes, a computer controlled *XYZ*-translation stage system (CONEXMFACC, Newport Co., Irvine, California), and a Thermo LTQ Orbitrap XL mass spectrometer (Thermo Scientific, Waltham, Massachusetts). A detailed description for the Single-probe fabrication and the experimental setup was reported in our previous studies.[51,57,71,100−102] Briefly, the Single-probe was fabricated by combining a laser-pulled (P-2000 Micropipette Laser Puller, Sutter Instrument Co., Novato, CA) dual-bore quartz needle (outer diameter (OD) 500 μm; inner diameter (ID) 127 μm, Friedrich & Dimmock, Inc., Millville, New Jersey) embedded with a fused silica capillary (OD 105 μm; ID 40 μm, Polymicro Technologies, Phoenix, Arizona) in one channel and a nano-ESI emitter, which was produced from the same fused silica capillary, in another channel. These three parts were sealed using UV curing resin (Light Cure Bonding Adhesive, Prime-Dent, Chicago, Illinois).

Glass coverslips containing cells were rinsed with fresh DMEM or RPMI medium (no FBS supplement) and placed on top of the *XYZ*−translational stage system for the Single-probe SCMS measurement. The targeted single cells were selected for analysis by carefully adjusting the stage system to locate the single cell. The entire process is monitored and guided by a digital microscope (Figure S2). Due to the small size of cells, the Single-probe was designed to have small tip sizes (~9 μm) to accurately analyze one cell at a time. The organic solvent (acetonitrile with 0.1% formic acid) was delivered through the fused silica capillary to extract cellular contents, followed by ionization via the nano-ESI emitter and real-time SCMS analysis (Figure S2). The Single-probe SCMS was conducted with the following parameters: 200 nL/min flow rate; mass resolution, 60 000; +4.5 kV ionization voltage; 1 microscan; 100 ms max injection time. MS/MS experiments of single cells were conducted under the following parameters: CID mode, 200 nL/min flow rate; mass resolution 60 000; +4.5 kV ionization voltage; 3 microscan; 500 ms max injection time.

SCMS Data Pretreatment and Statistical Analysis. The SCMS data pretreatment was performed using our previously established protocol.[47,51] SCMS data were exported with peaks (m/z values and their relative intensities) generated by Thermo Xcalibur Qual Browser 3.0 (Thermo Scientific, Waltham, Massachusetts). Noise subtraction was performed to remove peaks with relative intensity $<3 \times 10^3$. Background signals generated from the organic solvent and cell culture medium were subtracted using an in-house R script as described in our prior work.[62,103] Normalization of the ion intensities to the total ion current (TIC) was conducted prior to peak alignment. The normalized data were uploaded to an online bioinformatics tool, Geena2,[104] for peak alignment (with a mass tolerance of 10 ppm) and subsequent analysis. Geena2 parameters were as follows: analysis range from 150 to 1500 m/z, maximum number of isotopic replicas (3), maximum delta between isotopic peaks (0.01 Da), maximum delta for aligning replicates (0.01 Da), and maximum delta for aligning average spectra (0.01 Da). After the peak alignment, missing values (50%) were removed using an in-house Python script. The pretreated SCMS data were used for principal

https://doi.org/10.1021/acs.analchem.4c02038
Anal. Chem. 2024, 96, 19238−19247

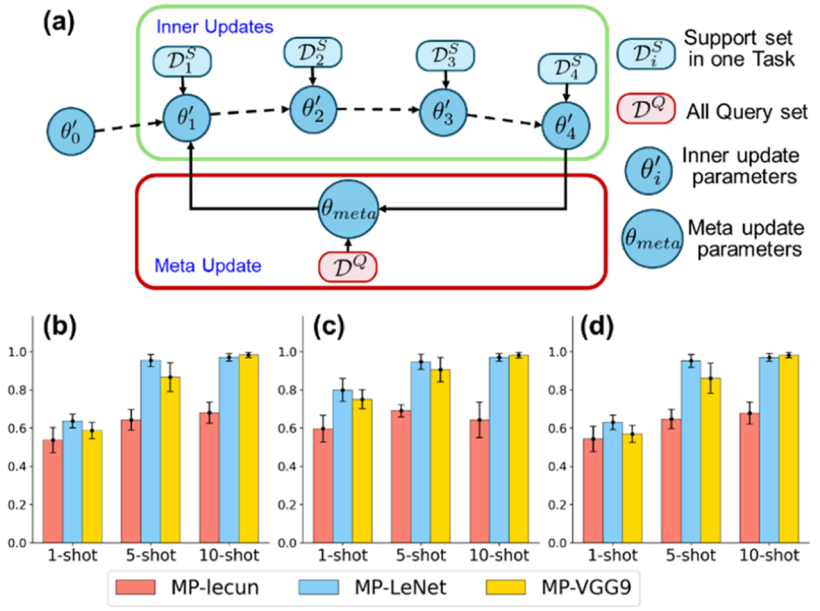

Figure 2. Training and evaluating MetaPhenotype (MP) constructed using three different architectures (LeCun, LeNet, and VGG9) with a total of 50 epochs. (a) Training workflow for one epoch. The prediction accuracy of MP models was represented as (b) area under the receiver operating characteristic (AUROC) curve, (c) F-1 score, and (d) accuracy for test set three distinct MP's architectures. The reported results are shown as an average of 10 separated trainings with 1-, 5-, and 10-shot.

component analysis (PCA) using MetaboAnalyst 6.0.[105] To obtain ions with significantly different abundances (i.e., fold change (FC) $\geq$ 2.0, and adjusted p-value threshold $\leq$ 0.05) among primary/metastatic cell groups, volcano plots[106] were generated.

Design of MetaPhenotype. *Data Set for MAML-Based MetaPhenotype Training.* Four different cell lines (i.e., IGR39, IGR37, WM115, and WM266-4) were used as models in our studies. Both treated (by vemurafenib) and untreated (control) cells in each cell line were analyzed. The SCMS data collected from these cell line models were used to train and test our meta-learning model.

In the meta-learning stage, we used SCMS data (m/z peaks; normalized intensity I; phenotype label y) from a pair of control cells, IGR39 and IGR37, as the meta-training data set to build MetaPhenotype. These SCMS data were split into the training set $(m/z_i, y_i)^{\text{training}}$, validation set $(m/z_i, y_i)^{\text{validation}}$, and test set $(m/z_i, y_i)^{\text{test}}$. Each training data point consists of the m/z (MS peaks), I (normalized intensity), and y (phenotype label as primary or metastatic) of an IGR39 cell and those of an IGR37 cell. These training data points were further split into support and query sets. We employed a K-shot learning setting to train the MetaPhenotype. In each task, 1, 5, or 10 samples were randomly picked from the support set, leading to 1-shot, 5-shot, or 10-shot models (Figure 2). For example, 1-shot model indicates that one pair of SCMS data (i.e., from one primary and one metastatic cell) was used to train the model. Training, validation, and the test set consisted of multiple tasks.

In the adaptation stage, we adapted the trained MetaPhenotype using the SCMS data obtained from other cell groups (i.e., drug-treated IGR39/IGR37, control WM115/WM266-4, and drug-treated WM115/WM266-4). Since these three pairs of cell lines were not used for MetaPhenotype training, this step served to assess the transferability of the model developed during the meta-learning stage. As in the meta-learning stage, 1- or 5-shot model adaptation was carried out using the support/query set and then further evaluated using other samples.

The selection of a suitable algorithm of the backbone, which is the network used for feature extraction, is critical for the performance of a machine learning model. We compared the performance of MetaPhenotype and other three popular machine learning algorithms, namely MAML backbone algorithm LeNet,[107−110] random forest (RF[111−113]), and support vector machine (SVM[66,114−117]). To make a fair comparison, the training, validation, and test sets were the same for each algorithm.

MetaPhenotype Framework. In the meta-learning model, we utilized MAML algorithm[86] that can be rapidly adapted to new tasks of determining cell phenotype distribution.

$$\theta_i' \leftarrow \theta_{\text{meta}} - \alpha \nabla_{\theta_{\text{meta}}} \mathcal{L}(\theta_{\text{meta}}, \mathcal{D}_i^S) \tag{1}$$

where, α is the learning rate for inner loops, D_i^S is the n-shot support data set for task i, and L is the loss function (defined in eq 3). After a fixed number of cycles (5 cycles in this work) in the inner loop, the meta parameter optimization switches to the outer loop. There, the meta parameter θ were updated as follows

$$\theta_{\text{meta}} \leftarrow \theta_{\text{meta}} - \beta \nabla_{\theta_{\text{meta}}} \mathcal{L}(\theta_i', \mathcal{D}^Q) \tag{2}$$

where, β is the learning rate for outer loops and D^Q is an n-shot query data set.

Because there are two types of cells in each task, the binary cross entropy was used as the loss function

$$L_{T_i}(f_\phi) = \sum_{x^{(j)}, y^{(j)} \sim T_i} y^{(j)} \log f_\phi(x^{(j)}) + (1 - y^{(j)}) \log(1 - f_\phi(x^{(j)})) \tag{3}$$

https://doi.org/10.1021/acs.analchem.4c02038
Anal. Chem. 2024, 96, 19238−19247

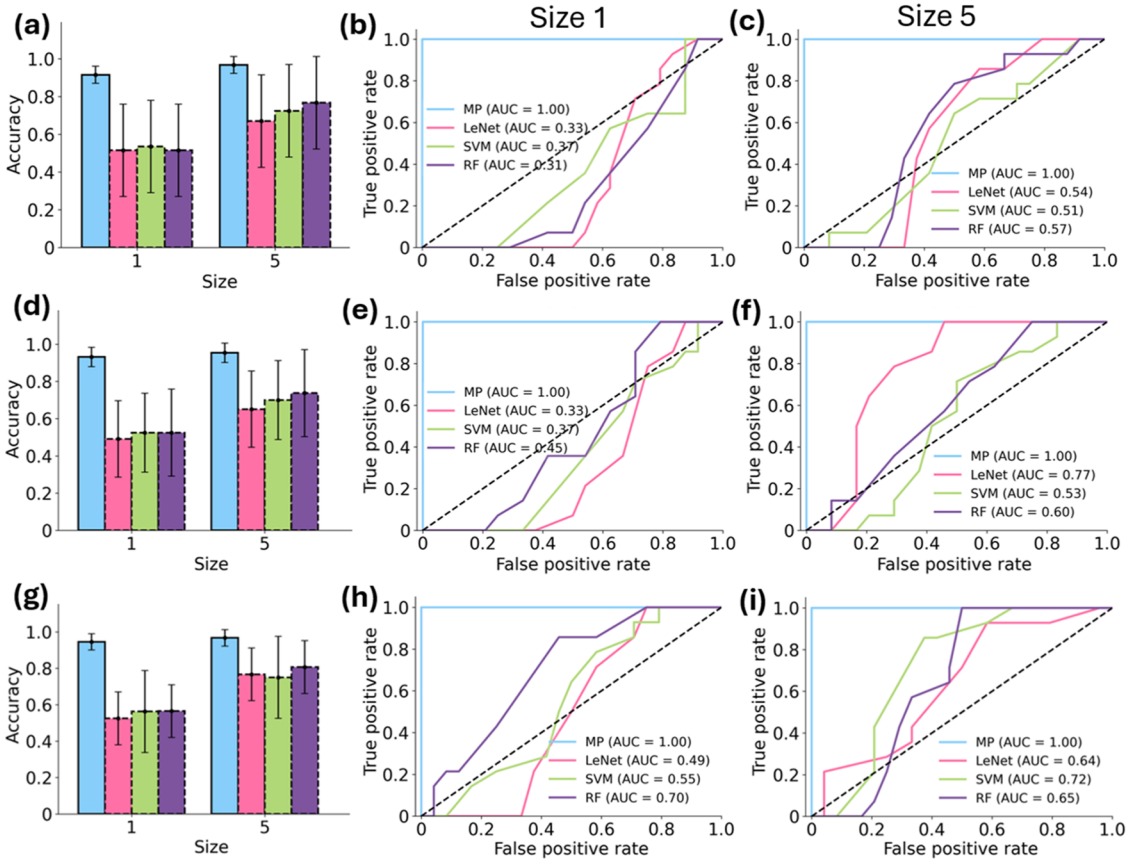

Figure 3. Meta-evaluation of the model transferability of MetaPhenotype. The performance of MetaPhenotype, classic convolutional neural network (CNN, LeNet as architecture), SVM, and RF were evaluated for their classification accuracy and AUROC of different cell models, including (a−c) untreated WM115/WM266-4, (d−f) treated WM115/WM266-4, and (g−i) treated IGR39/IGR37. Calculations of the accuracy and AUROC were conducted using two training set sizes (1 and 5).

where, x is the normalized m/z data, y is the cell phenotype for support/query data points for the specific task T_i, and f_ϕ represents the output of the MetaPhenotype model from input $x^{(j)}$.

Machine Learning Training Details. To test the influence of CNN architectures on MetaPhenotype performance, each of three common architectures (i.e., Lecun, LeNet, and VGG9) was separately used to construct the backbone of the MetaPhenotype. These CNN architectures share the same hyperparameters.[99] ReLU was used as the activation function in the convolution layers, whereas the sigmoid function was used in the output layer for binary classification (i.e., primary or metastatic cells). All models were trained by SGD (stochastic gradient descent) with Adam optimizer and a constant learning rate of 10^{-3}. For comparison, we trained MetaPhenotype with 1, 5, and 10-shot scenarios. The total task number for different shot training is summarized in Table S2. To measure the classification performance of MetaPhenotype models, we computed the area under the receiver operating characteristic curve (AUROC), F-1 score, and prediction accuracy after 50 total epochs of training (Figure 2). For each type of model, the binary classification accuracy is an average of over 10 independent iterations.

RESULT AND DISCUSSION

Single-Probe SCMS Results. In the current study, we employed the Single-probe SCMS technique to investigate the metabolomics of primary and metastatic melanoma pairs. The metabolic profiles obtained were then utilized for cell phenotype classification using MetaPhenotype. To assess the model's reliability under the influence of microenvironmental shifts, vemurafenib was used as a stimulus for cell treatment. We analyzed four different pairs of primary/metastatic melanoma cells: untreated IGR39/IGR37, treated IGR39/IGR37, untreated WM115/WM266-4, and treated WM115/WM266-4 (Figures S3−S6). The number of cells analyzed in each group using SCMS experiments is summarized in Table S2. Since our Single-probe SCMS technique has a relatively lower throughput for analysis of live cells, only 27−58 cells in each group were measured, generating a suitable case study using MAML-based machine learning method.

The online databases (METLIN[118] and HMDB[119]) were used to tentatively label the detected species based upon their m/z values. Detailed structure identification of metabolites, such as MS/MS analysis at the single-cell level or LC/MS measurement of cell lysate, offers valuable insights into facilitate the discovery of metabolite biomarkers and the understanding of drug resistance mechanisms. We labeled and identified significant peaks (see Determination of Significant Peaks) such as triglycerides (TG), ceramides (Cer), sphingomyelin (SM), phosphatidylglycerol (PG), and phosphatidylethanolamine (PE) (Tables S4 and S5). These metabolites exhibited significantly different abundances between primary and metastatic cells, suggesting that they are potential metabolite biomarkers. By utilizing these significant peaks, we were able to prioritize metabolite

https://doi.org/10.1021/acs.analchem.4c02038
Anal. Chem. 2024, 96, 19238−19247

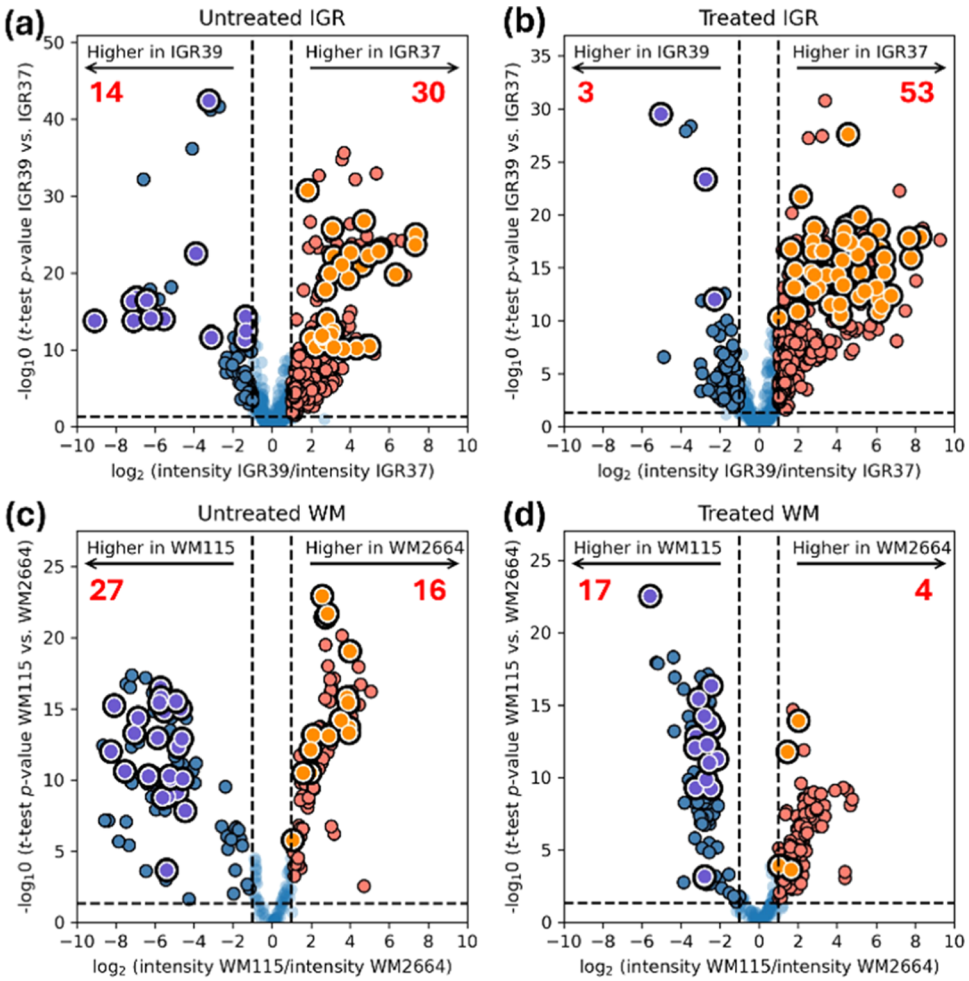

Figure 4. Using MetaPhenotype to reveal significant peaks contributing to cell phenotypes. Volcano plots were used to indicate differential metabolic profiles of primary and metastatic melanoma cells with and without vemurafenib treatment. The comparison was performed for (a) untreated IGR39/IGR37 (training set), (b) treated IGR39/IGR37, (c) untreated WM115/WM266-4, and (d) treated WM115/WM266-4 cells. Each dot represents a metabolite with a fold change (FC) > 2.0 and 0.05 false-discovery rate (FDR) adjusted *p*-value. Common significant peaks (numbers are shown) determined by both MetaPhenotype and volcano plots are illustrated as highlighted dots.

biomarkers without relying on tests of significance, including the Student's *t* test and *p*-value. These potential biomarkers can then be identified in a target analysis. However, molecular identification of these potential biomarkers has no significant impact on the prediction performance of the MAML machine learning model; further molecular identification will be pursued in follow-up work.

Meta-Training. Our primary goal is to develop a new machine learning model for cell phenotype classification using limited amounts of SCMS data. We constructed an MAML-based model, MetaPhenotype, and trained it using SCMS data acquired from IRG39 (primary melanoma) and IGR37 (metastatic melanoma) cells without drug treatment. Inspired by the recent work of Seddiki et al., in which three different types of 1D-CNN blocks (i.e., Lecun, LetNet, and VGG9) were used to MS data analysis,[99] we used these three architectures to construct MetaPhenotype. We then compared their prediction accuracies using the two test sets. These three algorithms contain different numbers of CNN blocks: Lecun, LeNet, and VGG9 have four, five, and nine blocks, respectively. To evaluate the performance of the MetaPhenotype model, the final results were reported in three different metrics: AUROC score, F1 score, and accuracy. The AUROC score represents the performance of MetaPhenotype under different thresholds. F1 score reflects the combined precision and recall scores of the model. Accuracy is used to evaluate the accuracy of the model classification. To evaluate the MetaPhenotype model, we used the 1-shot, 5-shot, and 10-shot settings to train MetaPhenotype. The meta-evaluation results indicate that LeNet and VGG9 had comparable performance (i.e., with similar results from all three metrics) for all three different shot settings. However, with the LeNet-based model outperforming the VGG9 model in the 5-shot setting, the LeNet algorithm was selected as the backbone of MetaPhenotype due to its efficiency and relatively higher accuracy.

Meta-Evaluation of Model Transferability. In the meta-evaluation processes, we sampled three types of melanoma cancer cells (treated IGR39/IGR37, untreated WM115/WM266-4, and treated WM115/WM266-4) unseen to the trained MetaPhenotype model to categorize each cell's phenotype into either primary or metastatic cell. The transferability of this model can be reflected in the test results using these new data. As shown in Figure 3, the prediction accuracy of MetaPhenotype for WM (both control and treated) and IGR (treated) cells were over 90% with only five steps of training.

https://doi.org/10.1021/acs.analchem.4c02038
Anal. Chem. 2024, 96, 19238−19247

Comparison with Other Methods. We compared the performance of MetaPhenotype with other common machine learning methods, including support vector machine (SVM), random forest (RF), LeNet (MetaPhenotype backbone), and ANN. In terms of the prediction accuracy metrics, the MetaPhenotype model achieved an accuracy over 95%. However, SVM, RF, and LeNet displayed a < 60% accuracy (Figure 3). MetaPhenotype also outperformed these three algorithms in terms of AUROC: the AUROC value is 1.0 for MetaPhenotype with both training set sizes, whereas this value ranges between 0.4 and 0.6 for the other three ML algorithms. Although ANN provided excellent accuracy (92%) for treated IGR39/IGR37 cells, poor performance was observed when analyzing the untreated (66%) and treated (29%) WM115/WM266-4 cells (Table S6 and Figure S7), indicating model overfitting likely due to limited data size. We also tested two cluster analytical methods, hierarchical clustering analysis (HCA) and PCA, commonly used in SCMS data analysis. Both methods are unsupervised and require no model training. HCA provided acceptable accuracy (72%) for treated IGR39/IGR37 cells but poor results for untreated (7%) and treated (14%) WM115/WM266-4 cells (Table S7). As a dimensionality reduction and visualization tool, PCA is not generally used by itself to provide prediction accuracy, but its performance of grouping data can be evaluated by using the score plot (Figure S8). Compared with WM115/WM266-4 cell pair, which were well separated by PCA, metabolites' profiles of IGR39/IGR37 cell pair significantly overlapped. Thus, PCA cannot effectively discriminate phenotypical cells with relatively high similarities in metabolomic profiles such as IGR39/IGR37 cells. Our results indicate that MetaPhenotype surpassed all other methods and had superior performance for cell phenotype prediction in the current studies.

Determination of Significant Peaks. Volcano plots are commonly used to discover species significantly differing between two groups of samples. In the current work, volcano plots were generated to reveal differential metabolic profiles between primary and metastatic melanoma cells, for both control and vemurafenib treated groups, through pairwise comparison (Figure 4). A large number of differential species are shown in the volcano plots. These species were determined by the FDR-adjusted p-value and fold change, which generally require an adequate amount of data for statistically meaningful explanation. In fact, MetaPhenotype can be used to capture significant peaks, which are a small number of essential species critical for determining cell phenotypes. If manually removing a certain peak from the SCMS data set in the MetaPhenotype model resulted in a decrease of ≥1% in the classification accuracy of cell phenotype, this ion will be regarded as a significant peak. These essential species were illustrated on volcano plot as bold dots, which are in common with those discovered using volcano plots, in Figure 4. We did not investigate the biological significance of these species, as this task is beyond the scope of the current work.

For IGR cells without drug treatment, 14 and 30 significant peaks, which were the common features illustrated on the volcano plots, were observed in the primary (IGR39) and metastatic cells (IGR37) cells (Figure 4a). Upon drug treatment, IGR39 and IGR37 cells rendered 3 and 53 significant peaks, respectively (Figure 4b). We performed similar analyses for WM cell lines (WM115 and WM266-4), and significant peaks are illustrated in Figure 4c,d for cells with and without drug treatment, respectively. Clearly, the numbers of significant peaks were much smaller than those reported from volcano plots, indicating that MetaPhenotype could capture a small number of essential species that are critical for discriminating cell phenotypes. Instead of investigating all potential candidates provided by traditional methods (e.g., volcano plot and t test), MetaPhenotype allows for more focused studies of far fewer molecules, potentially improving our understanding of unique molecular features and metabolism of phenotypic cells.

Limitations of MAML-Based Machine Learning Models. MetaPhenotype was constructed based on the MAML machine learning model. While this MAML-based model worked reasonably well here, we note a few weaknesses. First, due to the need for multiple gradient descent steps in the inner loop and backpropagation through these updates in the outer loop, it can be memory and computationally intensive for larger samples. Second, the MAML model is sensitive to its hyperparameters, requiring careful tuning of learning rates and the number of updates. Finally, MAML works less well in nonstationary environments, where task distributions change over time and can become numerically unstable due to the use of second-order derivatives. Given these challenges, it would be desirable to go beyond MAML, a foundational approach in meta-learning, and test various techniques addressing its limitations.[120−123]

CONCLUSIONS

In the present study, we developed a meta-learning-based model termed MetaPhenotype. Utilizing the Single-probe SCMS technique, we analyzed melanoma cell lines with primary and metastatic phenotypes before and after drug treatment. SCMS metabolomics data of one cell pair were used as the training and evaluation data sets, and the trained MetaPhenotype model was then used to analyze the remaining data. MetaPhenotype was demonstrated to show rapid adaptation and high transferability, providing high prediction accuracies of cell phenotypes using only small sample sizes. In addition, MetaPhenotype allows selection of small numbers of essential species critical for classification of cell phenotypes. It is worth noting that applications of MetaPhenotype are not limited to analyzing data for the primary/metastatic melanoma cell lines obtained using our Single-probe SCMS experimental setup. This software tool can be potentially used to analyze the metabolomics data acquired from other SCMS experimental platforms and cell systems.

ASSOCIATED CONTENT

Data Availability Statement

Source code of MetaPhenotype and example data are available on GitHub: https://github.com/songyuan93/MetaPhenotype. Raw data of the Single-probe SCMS experiments can be obtained from the MassIVE database (MSV000095551). Source code of ANN model: https://github.com/dandandan001/Single_cell_MS_ANN_classify.

Supporting Information

The Supporting Information is available free of charge at https://pubs.acs.org/doi/10.1021/acs.analchem.4c02038.

Experimental details of cell line model; data set splitting in MetaPhenotype; algorithm in MetaPhenotype; tables of tentative labels of metabolites; significant peaks identified using MS/MS identification in single cells; tables of ANN and HCA results; microscopic images of

https://doi.org/10.1021/acs.analchem.4c02038
Anal. Chem. 2024, 96, 19238−19247

primary/metastatic cells with and without drug treatment; single-probe SCMS setup; representative mass spectra; ANN training and validation; PCA results; Python and R scripts (PDF)

AUTHOR INFORMATION

Corresponding Authors

Yihan Shao − *Department of Chemistry and Biochemistry, University of Oklahoma, Norman, Oklahoma 73019, United States*; orcid.org/0000-0001-9337-341X; Email: Yihan.Shao@ou.edu

Zhibo Yang − *Department of Chemistry and Biochemistry, University of Oklahoma, Norman, Oklahoma 73019, United States*; orcid.org/0000-0003-0370-7450; Email: Zhibo.Yang@ou.edu

Authors

Songyuan Yao − *Department of Chemistry and Biochemistry, University of Oklahoma, Norman, Oklahoma 73019, United States*

Tra D. Nguyen − *Department of Chemistry and Biochemistry, University of Oklahoma, Norman, Oklahoma 73019, United States*

Yunpeng Lan − *Department of Chemistry and Biochemistry, University of Oklahoma, Norman, Oklahoma 73019, United States*

Wen Yang − *Stephenson School of Biomedical Engineering, University of Oklahoma, Norman, Oklahoma 73019, United States*; orcid.org/0000-0001-9206-0868

Dan Chen − *Department of Chemistry and Biochemistry, University of Oklahoma, Norman, Oklahoma 73019, United States*

Complete contact information is available at: https://pubs.acs.org/10.1021/acs.analchem.4c02038

Author Contributions

[§]S.Y., T.D.N., and Y.L. contributed equally to this paper.

Notes

The authors declare no competing financial interest.

ACKNOWLEDGMENTS

This work was supported by funds from National Science Foundation 2305182 (Z.Y.), National Institutes of Health R01AI177469 (Z.Y.) and R01GM135392 (Y.S.), and the University of Oklahoma's Office of the Vice President for Research and Partnerships.

REFERENCES

(1) Waks, A. G.; Winer, E. P. *Jama* **2019**, *321* (3), 288−300.
(2) Zugazagoitia, J.; Guedes, C.; Ponce, S.; Ferrer, I.; Molina-Pinelo, S.; Paz-Ares, L. *Clin. Ther.* **2016**, *38* (7), 1551−1566.
(3) Bertucci, F.; Birnbaum, D. *J. Biol.* **2008**, *7*, 1−4.
(4) Katenkamp, D. *Pathology-Res. Pract.* **1988**, *183* (6), 698−705.
(5) Saha, K.; Pollock, J. F.; Schaffer, D. V.; Healy, K. E. *Curr. Opin. Chem. Biol.* **2007**, *11* (4), 381−387.
(6) Bhatia, S. N.; Balis, U.; Yarmush, M.; Toner, M. *FASEB J.* **1999**, *13* (14), 1883−1900.
(7) Gay, L.; Baker, A.-M.; Graham, T. A. *F1000Research* **2016**, *5*, 238 DOI: 10.12688/f1000research.7210.1.
(8) Shackleton, M.; Quintana, E.; Fearon, E. R.; Morrison, S. J. *Cell* **2009**, *138* (5), 822−829.
(9) Jacquemin, V.; Antoine, M.; Dom, G.; Detours, V.; Maenhaut, C.; Dumont, J. E. *Cancers* **2022**, *14* (2), 280.
(10) Rognoni, E.; Watt, F. M. *Trends Cell Biol.* **2018**, *28* (9), 709−722.
(11) Brooks, M. D.; Burness, M. L.; Wicha, M. S. *Cell Stem Cell* **2015**, *17* (3), 260−271.
(12) Rivenbark, A. G.; O'Connor, S. M.; Coleman, W. B. *Am. J. Pathol.* **2013**, *183* (4), 1113−1124.
(13) Turner, N. C.; Reis-Filho, J. S. *Lancet Oncol.* **2012**, *13* (4), e178−e185.
(14) Zbytek, B.; Carlson, J. A.; Granese, J.; Ross, J.; Mihm, M.; Slominski, A. *Expert Rev. Dermatol.* **2008**, *3* (5), 569−585.
(15) Damsky, W. E.; Theodosakis, N.; Bosenberg, M. *Oncogene* **2014**, *33* (19), 2413−2422.
(16) Heath, J. R.; Ribas, A.; Mischel, P. S. *Nat. Rev. Drug Discovery* **2016**, *15* (3), 204−216.
(17) Sun, Y. H.; Wu, Y.-L.; Liao, B.-Y. *J. Biomed. Sci.* **2023**, *30* (1), 58.
(18) Tang, D. G. *Cell Res.* **2012**, *22* (3), 457−472.
(19) Papalexi, E.; Satija, R. *Nat. Rev. Immunol.* **2018**, *18* (1), 35−45.
(20) Yu, Z.; Huang, M.; Clowers, B. H. *Clin. Mass Spectrom.* **2018**, *10*, 16−24.
(21) Johnson, C. H.; Santidrian, A. F.; LeBoeuf, S. E.; Kurczy, M. E.; Rattray, N. J. W.; Rattray, Z.; Warth, B.; Ritland, M.; Hoang, L. T.; Loriot, C.; et al. *Cancer Metab* **2017**, *5*, 9. From NLM.
(22) Brar, G.; Blais, E. M.; Joseph Bender, R.; Brody, J. R.; Sohal, D.; Madhavan, S.; Picozzi, V. J.; Hendifar, A. E.; Chung, V. M.; Halverson, D.; et al. *Br. J. Cancer* **2019**, *121* (3), 264−270.
(23) Kim, H. M.; Jung, W. H.; Koo, J. S. *J. Transl. Med.* **2014**, *12* (1), 354.
(24) May, C. A. *Histochem. Cell Biol.* **1999**, *112* (5), 381−386.
(25) Hatina, J.; Boesch, M.; Sopper, S.; Kripnerova, M.; Wolf, D.; Reimer, D.; Marth, C.; Zeimet, A. G. *Stem Cells Heterog. Cancer* **2019**, *1139*, 201−221.
(26) Aird, W. C. *Cold Spring Harbor Perspect. Med.* **2012**, *2* (1), No. a006429.
(27) Darzynkiewicz, Z.; Crissman, H.; Traganos, F.; Steinkamp, J. *J. Cell. Physiol.* **1982**, *113* (3), 465−474.
(28) Zhang, A.; Sun, H.; Xu, H.; Qiu, S.; Wang, X. *OMICS: J. Integr. Biol.* **2013**, *17* (10), 495−501.
(29) Volkova, S.; Matos, M. R.; Mattanovich, M.; Marín de Mas, I. *Metabolites* **2020**, *10* (8), 303.
(30) Lan, Y.; Zou, Z.; Yang, Z. *TrAC, Trends Anal. Chem.* **2024**, *174*, No. 117657.
(31) Zhang, L. W.; Vertes, A. *Angew. Chem., Int. Ed.* **2018**, *57* (17), 4466−4477.
(32) Rubakhin, S. S.; Lanni, E. J.; Sweedler, J. V. *Curr. Opin. Biotechnol.* **2013**, *24* (1), 95−104. From NLM.
(33) Amantonico, A.; Urban, P. L.; Zenobi, R. *Anal. Bioanal. Chem.* **2010**, *398* (6), 2493−2504. From NLM.
(34) Rubakhin, S. S.; Lanni, E. J.; Sweedler, J. V. *Curr. Opin. Biotechnol.* **2013**, *24* (1), 95−104.
(35) Armbrecht, L.; Dittrich, P. S. *Anal. Chem.* **2017**, *89* (1), 2−21.
(36) Chen, X.; Peng, Z.; Yang, Z. *Chem. Sci.* **2022**, *13* (22), 6687−6695.
(37) Amantonico, A.; Urban, P. L.; Zenobi, R. *Anal. Bioanal. Chem.* **2010**, *398* (6), 2493−2504.
(38) Nguyen, Q. H.; Lukowski, S. W.; Chiu, H. S.; Senabouth, A.; Bruxner, T. J.; Christ, A. N.; Palpant, N. J.; Powell, J. E. *Genome Res.* **2018**, *28* (7), 1053−1066.
(39) Cheng, S.; Pei, Y.; He, L.; Peng, G.; Reinius, B.; Tam, P. P.; Jing, N.; Deng, Q. *Cell Rep.* **2019**, *26* (10), 2593−2607.e2593.
(40) Gupta, R. K.; Kuznicki, J. *Cells* **2020**, *9* (8), 1751.
(41) Lo, P. K.; Zhou, Q. Emerging techniques in single-cell epigenomics and their applications to cancer research *J. Clin. Genom.* 2018; Vol. *1* 1 DOI: 10.4172/jcg.1000103.
(42) Qi, Z.; Barrett, T.; Parikh, A. S.; Tirosh, I.; Puram, S. V. *Oral Oncol.* **2019**, *99*, No. 104441.
(43) Evrony, G. D.; Hinch, A. G.; Luo, C. *Annu. Rev. Genomics Hum. Genet.* **2021**, *22* (1), 171−197.

(44) Piltti, K. M.; Cummings, B. J.; Carta, K.; Manughian-Peter, A.; Worne, C. L.; Singh, K.; Ong, D.; Maksymyuk, Y.; Khine, M.; Anderson, A. J. *Methods* **2018**, *133*, 81−90.
(45) Düssmann, H.; Perez-Alvarez, S.; Anilkumar, U.; Papkovsky, D. B.; Prehn, J. H. M. *Cell Death Dis.* **2017**, *8* (6), e2853.
(46) Rennerfeldt, D. A.; Raminhos, J. S.; Leff, S. M.; Manning, P.; Van Vliet, K. J. *PLoS One* **2019**, *14* (4), No. e0213452.
(47) Pan, N.; Rao, W.; Kothapalli, N. R.; Liu, R.; Burgett, A. W. G.; Yang, Z. *Anal. Chem.* **2014**, *86* (19), 9376−9380.
(48) Rao, W.; Pan, N.; Yang, Z. *J. Visualized Exp.: JoVE* **2016**, No. 112, No. e53911.
(49) Sun, M.; Yang, Z. *Anal. Chem.* **2019**, *91* (3), 2384−2391.
(50) Sun, M.; Yang, Z. B.; Wawrik, B. *Front. Plant Sci.* **2018**, *9*, 571.
(51) Nguyen, T. D.; Lan, Y.; Kane, S. S.; Haffner, J. J.; Liu, R.; McCall, L.-I.; Yang, Z. *Anal. Chem.* **2022**, *94* (30), 10567−10572.
(52) Chen, X.; Sun, M.; Yang, Z. *Anal. Chim. Acta* **2022**, *1201*, No. 339621. From NLM Medline.
(53) Sun, M.; Chen, X.; Yang, Z. *Anal. Chim. Acta* **2022**, *1206*, No. 339761. From NLM Medline.
(54) Liu, R.; Sun, M.; Zhang, G.; Lan, Y.; Yang, Z. *Anal. Chim. Acta* **2019**, *1092*, 42−48.
(55) Liu, R.; Zhang, G.; Yang, Z. *Chem. Commun.* **2019**, *55* (5), 616−619.
(56) Liu, M.; Zhang, Y.; Yang, J.; Cui, X.; Zhou, Z.; Zhan, H.; Ding, K.; Tian, X.; Yang, Z.; Fung, K. A.; et al. *Gastroenterology* **2020**, *158* (3), 679−692 e671.
(57) Pan, N.; Standke, S. J.; Kothapalli, N. R.; Sun, M.; Bensen, R. C.; Burgett, A. W. G.; Yang, Z. *Anal. Chem.* **2019**, *91* (14), 9018−9024.
(58) Bensen, R. C.; Standke, S. J.; Colby, D. H.; Kothapalli, N. R.; Le-McClain, A. T.; Patten, M. A.; Tripathi, A.; Heinlen, J. E.; Yang, Z.; Burgett, A. W. G. *ACS Pharmacol. Transl. Sci.* **2021**, *4* (1), 96−100.
(59) Lan, Y.; Chen, X.; Yang, Z. *Anal. Chem.* **2023**, *95* (51), 18871−18879.
(60) Yue, W.; Wang, Z.; Chen, H.; Payne, A.; Liu, X. *Designs* **2018**, *2* (2), 13.
(61) Iqbal, M. J.; Javed, Z.; Sadia, H.; Qureshi, I. A.; Irshad, A.; Ahmed, R.; Malik, K.; Raza, S.; Abbas, A.; Pezzani, R.; Sharifi-Rad, J. *Cancer Cell Int.* **2021**, *21* (1), 270.
(62) Liu, R.; Zhang, G.; Sun, M.; Pan, X.; Yang, Z. *Anal. Chim. Acta* **2019**, *1064*, 71−79.
(63) Kourou, K.; Exarchos, T. P.; Exarchos, K. P.; Karamouzis, M. V.; Fotiadis, D. I. *Comput. Struct. Biotechnol. J.* **2015**, *13*, 8−17.
(64) Ferroni, P.; Zanzotto, F. M.; Riondino, S.; Scarpato, N.; Guadagni, F.; Roselli, M. *Cancers* **2019**, *11* (3), 328.
(65) Gertrudes, J. C.; Maltarollo, V. G.; Silva, R.; Oliveira, P. R.; Honorio, K. M.; Da Silva, A. *Curr. Med. Chem.* **2012**, *19* (25), 4289−4297.
(66) Burbidge, R.; Trotter, M.; Buxton, B.; Holden, S. *Comput. Chem.* **2001**, *26* (1), 5−14.
(67) Mouchlis, V. D.; Afantitis, A.; Serra, A.; Fratello, M.; Papadiamantis, A. G.; Aidinis, V.; Lynch, I.; Greco, D.; Melagraki, G. *Int. J. Mol. Sci.* **2021**, *22* (4), 1676.
(68) Liebal, U. W.; Phan, A. N. T.; Sudhakar, M.; Raman, K.; Blank, L. M. *Metabolites* **2020**, *10* (6), 243.
(69) Zou, Z.; Peng, Z.; Bhusal, D.; Wije Munige, S.; Yang, Z. *Anal. Chim. Acta* **2024**, *1325*, No. 343124.
(70) Liu, R. M.; Yang, Z. B. *Anal. Chim. Acta* **2021**, *1143*, 124−134.
(71) Tian, X.; Zhang, G.; Zou, Z.; Yang, Z. *Anal. Chem.* **2019**, *91* (9), 5802−5809.
(72) Tian, X.; Zhang, G.; Shao, Y.; Yang, Z. *Anal. Chim. Acta* **2018**, *1037*, 211−219.
(73) Maseda, F.; Cang, Z.; Nie, Q. *Front. Genet.* **2021**, *12*, No. 636743.
(74) Peralta, D.; Saeys, Y. *Appl. Soft Comput.* **2020**, *93*, No. 106421.
(75) Papagiannopoulou, C.; Parchen, R.; Rubbens, P.; Waegeman, W. *Anal. Chem.* **2020**, *92* (11), 7523−7531.
(76) Do, T. D.; Comi, T. J.; Dunham, S. J.; Rubakhin, S. S.; Sweedler, J. V. *Anal. Chem.* **2017**, *89* (5), 3078−3086.
(77) Xie, Y. R.; Castro, D. C.; Bell, S. E.; Rubakhin, S. S.; Sweedler, J. V. *Anal. Chem.* **2020**, *92* (13), 9338−9347.
(78) Portero, E. P.; Nemes, P. *Analyst* **2019**, *144* (3), 892−900.
(79) Bergman, H.-M.; Lanekoff, I. *Analyst* **2017**, *142* (19), 3639−3647.
(80) Abouleila, Y.; Onidani, K.; Ali, A.; Shoji, H.; Kawai, T.; Lim, C. T.; Kumar, V.; Okaya, S.; Kato, K.; Hiyama, E.; et al. *Cancer Sci.* **2019**, *110* (2), 697−706.
(81) Ying, X. *J. Phys.: Conf. Ser.* **2019**, *1168* (2), No. 022022.
(82) Parnami, A.; Lee, M. Learning from few examples: A summary of approaches to few-shot learning *arXiv preprint arXiv:2203.04291* 2022.
(83) Schaul, T.; Schmidhuber, J. *Scholarpedia* **2010**, *5* (6), No. 4650.
(84) Thrun, S.; Pratt, L. Learning to Learn: Introduction and Overview. In *Learning to Learn*; Kluwer Academic Publishers, 1998; pp 3−17.
(85) Thrun, S.; Pratt, L. *Learning to Learn: Introduction and Overview*; Kluwer Academic Publishers, 1998.
(86) Finn, C.; Abbeel, P.; Levine, S. Model-Agnostic Meta-Learning for Fast Adaptation of Deep Networks. In *Proceedings of the 34th International Conference on Machine Learning, Proceedings of Machine Learning Research* 2017.
(87) Raghu, A.; Raghu, M.; Bengio, S.; Vinyals, O. Rapid learning or feature reuse? towards understanding the effectiveness of maml *arXiv preprint arXiv:1909.09157* 2019.
(88) Yin, W. Meta-learning for few-shot natural language processing: A survey *arXiv preprint arXiv:2007.09604* 2020.
(89) Alet, F.; Lozano-Perez, T.; Kaelbling, L. P. Modular Meta-learning. In *Proceedings of The 2nd Conference on Robot Learning, Proceedings of Machine Learning Research* 2018.
(90) Kiranyaz, S.; Avci, O.; Abdeljaber, O.; Ince, T.; Gabbouj, M.; Inman, D. J. *Mech. Syst. Signal process.* **2021**, *151*, No. 107398.
(91) Kiranyaz, S.; Ince, T.; Abdeljaber, O.; Avci, O.; Gabbouj, M. 1-D Convolutional Neural Networks for Signal Processing Applications. In *ICASSP 2019−2019 IEEE International Conference on Acoustics, Speech and Signal Processing (ICASSP)*; IEEE, 2019; pp 8360−8364.
(92) Chen, C.-C.; Liu, Z.; Yang, G.; Wu, C.-C.; Ye, Q. *Electronics* **2021**, *10* (1), 59.
(93) Zhao, J.; Mao, X.; Chen, L. *Biomed. Signal Process. Control* **2019**, *47*, 312−323.
(94) Chang, P. D.; Kuoy, E.; Grinband, J.; Weinberg, B. D.; Thompson, M.; Homo, R.; Chen, J.; Abcede, H.; Shafie, M.; Sugrue, L.; et al. *Am. J. Neuroradiol.* **2018**, *39* (9), 1609−1616.
(95) Alakwaa, W.; Nassef, M.; Badr, A. *Int. J. Adv. Comput. Sci. Appl.* **2017**, *8* (8), 409 DOI: 10.14569/IJACSA.2017.080853.
(96) Maturana, D.; Scherer, S. Voxnet: A 3d Convolutional Neural Network for Real-time Object Recognition. In *2015 IEEE/RSJ. International Conference on Intelligent Robots and Systems (IROS)*; IEEE, 2015; pp 922−928.
(97) Li, Y.; Zhang, H.; Shen, Q. *Remote Sens.* **2017**, *9* (1), 67.
(98) Wu, Y.; Yang, F.; Liu, Y.; Zha, X.; Yuan, S. A comparison of 1-D and 2-D deep convolutional neural networks in ECG classification *arXiv preprint arXiv:1810.07088* 2018.
(99) Seddiki, K.; Saudemont, P.; Precioso, F.; Ogrinc, N.; Wisztorski, M.; Salzet, M.; Fournier, I.; Droit, A. *Nat. Commun.* **2020**, *11* (1), No. 5595.
(100) Liu, R.; Li, J.; Lan, Y.; Nguyen, T. D.; Chen, Y. A.; Yang, Z. *Anal. Chem.* **2023**, *95* (18), 7127−7133.
(101) Sun, M.; Tian, X.; Yang, Z. *Anal. Chem.* **2017**, *89* (17), 9069−9076.
(102) Standke, S. J.; Colby, D. H.; Bensen, R. C.; Burgett, A. W. G.; Yang, Z. *Anal. Chem.* **2019**, *91* (3), 1738−1742.
(103) Liu, R.; Pan, N.; Zhu, Y.; Yang, Z. *Anal. Chem.* **2018**, *90* (18), 11078−11085.
(104) Romano, P.; Profumo, A.; Rocco, M.; Mangerini, R.; Ferri, F.; Facchiano, A. *BMC Bioinf.* **2016**, *17* (4), 61.

(105) Ewald, J. D.; Zhou, G.; Lu, Y.; Kolic, J.; Ellis, C.; Johnson, J. D.; Macdonald, P. E.; Xia, J. *Nat. Protoc.* **2024**, *19*, 1467.
(106) Kumar, N.; Hoque, M. A.; Sugimoto, M. *BMC Bioinf.* **2018**, *19* (1), 128.
(107) Li, Z. W.; Liu, F.; Yang, W. J.; Peng, S. H.; Zhou, J. *IEEE Trans. Neural Networks Learn. Syst.* **2022**, *33* (12), 6999−7019.
(108) Wei, G. F.; Li, G.; Zhao, J.; He, A. X. *Sensors* **2019**, *19* (1), 217.
(109) Sakib, S.; Ahmed, N.; Kabir, A. J.; Ahmed, H. An Overview of Convolutional Neural Network: Its Architecture and Applications *Preprints* 2019.
(110) Kuo, C. C. J. *J. Visual Commun. Image Representation* **2016**, *41*, 406−413.
(111) Biau, G.; Scornet, E. *Test* **2016**, *25*, 197−227.
(112) Belgiu, M.; Drăgut, L. *ISPRS J. Photogramm. Remote Sens.* **2016**, *114*, 24−31.
(113) Breiman, L. *Mach. Learn.* **2001**, *45*, 5−32.
(114) Suthaharan, S.Support Vector Machine. In *Machine Learning Models and Algorithms for Big Data Classification: Thinking with Examples for Effective Learning*, Integrated Series in Information Systems; Springer, 2016; Vol. *36*, pp 207−235.
(115) Hearst, M. A.; Dumais, S. T.; Osuna, E.; Platt, J.; Scholkopf, B. *IEEE Intell. Syst. Appl.* **1998**, *13* (4), 18−28.
(116) Pisner, D. A.; Schnyer, D. M. Support Vector Machine. In *Mach. Learn.*; Elsevier, 2020; pp 101−121.
(117) Steinwart, I.; Christmann, A. *Support Vector Machines*; Springer Science & Business Media, 2008.
(118) Smith, C. A.; Maille, G. O.; Want, E. J.; Qin, C.; Trauger, S. A.; Brandon, T. R.; Custodio, D. E.; Abagyan, R.; Siuzdak, G. *Ther. Drug Monit.* **2005**, *27* (6), 747−751.
(119) Wishart, D. S.; Feunang, Y. D.; Marcu, A.; Guo, A. C.; Liang, K.; Vázquez-Fresno, R.; Sajed, T.; Johnson, D.; Li, C.; Karu, N.; et al. *Nucleic Acids Res.* **2018**, *46* (D1), D608−D617. From NLM.
(120) Antoniou, A.; Edwards, H.; Storkey, A. J.How to Train Your MAML. In *International Conference on Learning Representations* 2018; p abs/1810.09502.
(121) Yao, H.; Wei, Y.; Huang, J.; Li, Z. Hierarchically Structured Meta-learning. In *Proceedings of the 36th International Conference on Machine Learning, Proceedings of Machine Learning Research* 2019.
(122) Zintgraf, L.; Shiarli, K.; Kurin, V.; Hofmann, K.; Whiteson, S. Fast Context Adaptation via Meta-Learning. In *Proceedings of the 36th International Conference on Machine Learning, Proceedings of Machine Learning Research* 2019.
(123) Sun, Q.; Liu, Y.; Chua, T.-S.; Schiele, B. Meta-Transfer Learning for Few-Shot Learning *arXiv:1812.02391* 2018.

https://doi.org/10.1021/acs.analchem.4c02038
Anal. Chem. 2024, 96, 19238−19247